Extinction of oscillating populations

Naftali R. Smith[*] and Baruch Meerson[†]

Racah Institute of Physics, Hebrew University of Jerusalem, Jerusalem 91904, Israel
(Received 2 December 2015; published 7 March 2016)

Established populations often exhibit oscillations in their sizes that, in the deterministic theory, correspond to a limit cycle in the space of population sizes. If a population is isolated, the intrinsic stochasticity of elemental processes can ultimately bring it to extinction. Here we study extinction of oscillating populations in a stochastic version of the Rosenzweig-MacArthur predator-prey model. To this end we develop a WKB (Wentzel, Kramers and Brillouin) approximation to the master equation, employing the characteristic population size as the large parameter. Similar WKB theories have been developed previously in the context of population extinction from an attracting multipopulation fixed point. We evaluate the extinction rates and find the most probable paths to extinction from the limit cycle by applying Floquet theory to the dynamics of an effective four-dimensional WKB Hamiltonian. We show that the entropic barriers to extinction change in a nonanalytic way as the system passes through the Hopf bifurcation. We also study the subleading pre-exponential factors of the WKB approximation.

I. INTRODUCTION

Populations of individuals (of molecules, bacteria, animals, or even humans) can often be viewed as stochastic. The intrinsic (demographic) noise in the elemental processes governing these systems profoundly affects their dynamics. A dramatic example is the extinction of a long-lived isolated population resulting from a rare sequence of events when deaths prevail over births. Stochastic population dynamics in general, and population extinction in particular, have always been a part of population biology [1]. More recently they have attracted attention from statistical physicists, who view stochastic populations as a many-body system far from thermal equilibrium.

Extinction of single populations, driven by weak intrinsic noise, is by now well understood (see Refs. [1,2] and references therein). Extinction of one or more populations in long-lived multipopulation systems has also been extensively studied, assuming that, prior to extinction, the populations reside in the vicinity of an attracting fixed point in the space of population sizes [3–8,10,11]. Many coexisting populations, however, exhibit persistent oscillations in their sizes [12–16]. At the level of deterministic theory, these oscillations are usually described by a stable limit cycle in the space of population sizes. A well-known deterministic model that shows this feature—a variation of the celebrated Lotka-Volterra model [17,18]—is due to Rosenzweig and MacArthur [19]. Qualitatively similar models are used in epidemiology for a description of the dynamics of susceptible and infected populations during an epidemic [20–22] and for a description of the oscillatory dynamics of tumor growth [23,24]. Similar models describe oscillatory chemical reactions [25,26].

In this work we study extinction caused by the weak intrinsic noise of populations that exhibit a limit cycle in the space of population sizes. We evaluate the extinction rates and most likely routes to extinction in a stochastic version of the Rosenzweig-MacArthur (RMA) model that we propose.

We extend a WKB (after Wentzel, Kramers, and Brillouin) theory, previously developed for multiple populations residing in the vicinity of an attracting fixed point [3–8,10,11,27,28], to populations residing in the vicinity of a stable limit cycle. We show that the most likely routes to extinction in such systems are described by a new type of instantons—special phase trajectories of the underlying effective classical mechanics. In its leading order of the large-population-size expansion, the WKB theory yields the mean time to extinction (MTE) with an exponential accuracy that is up to a subleading prefactor. As we show here, our WKB results agree with numerical solutions of the master equation and with direct Monte Carlo simulations for this model up to a prefactor which is a subleading correction to the WKB result. We find that the entropic barrier to extinction behaves in a nonanalytic way at the Hopf bifurcation describing the birth of the limit cycle. Furthermore, we evaluate the subleading WKB prefactor numerically and find that it too changes its behavior at the Hopf bifurcation. We suggest theoretical arguments to explain these features. The results of this work can be extended to a whole class of models of isolated multiple populations which exhibit, at the deterministic level, a stable limit cycle.

Here is how the remainder of the paper is structured. In Sec. II we briefly recap the main properties of the deterministic RMA model and focus on the parameter region where the system exhibits a stable limit cycle in the space of population sizes. Section III deals with the stochastic version of the RMA model that we suggest. In particular, Sec. III A discusses the two routes to extinction that this model exhibits. In Sec. III B we present the master equation for the stochastic version of the RMA model and discuss its long-time properties. In Sec. III C we develop a WKB theory of population extinction in this model. We summarize our results in Sec. IV.

II. ROSENZWEIG-MACARTHUR MODEL: DETERMINISTIC DYNAMICS AND THE LIMIT CYCLE

We denote the population sizes of the predators and prey F (foxes) and R (rabbits), respectively, and assume that the population densities are homogeneous in space. The elemental processes and rates of the RMA model [19] are listed in Table I.

*naftalismith@gmail.com
†meerson@mail.huji.ac.il

TABLE I. Stochastic Rosenzweig-MacArthur model.

Process	Type of transition	Rate
Birth of rabbits	$R \to 2R$	aR
Predation and birth of foxes	$F + R \to 2F$	$\frac{sRF}{1+s\tau R}$
Death of foxes	$F \to 0$	F
Competition among rabbits	$2R \to R$	$\frac{R(R+1)}{2N}$

The rabbits reproduce at rate a and die, due to competition for resources, at rate $1/N$. The foxes die or leave at a constant per-capita rate, and the units of time are chosen such that this rate is equal to 1. The parameters s and τ are related to the predation rate as follows: For a small rabbit population R, the predation rate, sR, is proportional to R. For a very large rabbit population, the predation rate saturates at $1/\tau$ so as to describe satiation of the predators.

The deterministic equations for the RMA model are

$$\dot{R} = aR - \frac{1}{2N}R^2 - \frac{sRF}{1+s\tau R}, \tag{1}$$

$$\dot{F} = -F + \frac{sRF}{1+s\tau R}. \tag{2}$$

We assume that s scales with the system size as $s \propto 1/N$, where $N \gg 1$ is the scale of the population sizes. We introduce $x = R/N$, $y = F/N$, and $\sigma = sN = \mathcal{O}(1)$ and arrive at the rescaled equations

$$\dot{x} = ax - \frac{1}{2}x^2 - \frac{\sigma xy}{1+\sigma\tau x}, \quad \dot{y} = -y + \frac{\sigma xy}{1+\sigma\tau x}, \tag{3}$$

where all the quantities are assumed to be of order 1.

The deterministic RMA model has been extensively studied [19,29,30]. Here we recap the main results of these works that we need for our purposes. We are interested only in the regime of parameters

$$0 < \tau < 1, \quad \sigma > \sigma_0 = \frac{1}{2a(1-\tau)}, \tag{4}$$

when Eq. (3) have three fixed points describing nonnegative population sizes. The fixed point M_1 ($\bar{x}_1 = 0$, $\bar{y}_1 = 0$) corresponds to an empty system. It is a saddle point: attracting in the y direction (when there are no rabbits in the system) and repelling in the x direction. The fixed point M_2 ($\bar{x}_2 = 2a$, $\bar{y}_1 = 0$) describes a steady-state population of rabbits in the absence of foxes. It is also a saddle: attracting in the x direction (when there are no foxes) and repelling in a direction corresponding to the introduction of a few foxes into the system. The third fixed point M_3 ($\bar{x}_3, \bar{y}_3$), where

$$\bar{x}_3 = \frac{1}{\sigma(1-\tau)}, \quad \bar{y}_3 = \frac{2a\sigma(1-\tau)-1}{2\sigma^2(1-\tau)^2}, \tag{5}$$

describes the coexistence state of the rabbits and foxes. Its stability properties depend on the parameters: For

$$\sigma_0 < \sigma < \bar{\sigma} = \frac{\frac{a\tau(1+\tau)}{2(1-\tau)} - 1 - \sqrt{1+a\frac{1+\tau}{1-\tau}}}{a^2\tau^2 - 4a(1-\tau)}, \tag{6}$$
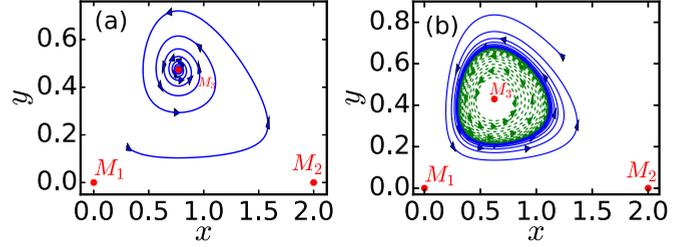
FIG. 1. Phase portrait of the deterministic RMA model, (3), for $a = 1$, $\tau = 0.5$, and two values of σ: (a) $\sigma = 2.6$, where M_3 is a stable focus, and (b) $\sigma = 3.2$, where M_3 is an unstable focus.

M_3 is a stable node. For

$$\bar{\sigma} < \sigma < \sigma^* = \frac{1+\tau}{2a\tau(1-\tau)}, \tag{7}$$

it is a stable focus. Finally, for $\sigma > \sigma^*$, M_3 is unstable, and a stable limit cycle appears around it. Noise-driven population extinction from a limit cycle has not been studied before. Therefore, in most of the paper we assume that $\sigma > \sigma^*$. A Hopf bifurcation occurs at $\sigma = \sigma^*$. Figure 1 shows the the behaviors of the deterministic model for $\bar{\sigma} < \sigma < \sigma^*$ [Fig. 1(a)] and for $\sigma > \sigma^*$ [Fig. 1(b)]. The characteristic time scale t_r of the deterministic dynamics is determined by the real part of the eigenvalues of the linear stability matrix at the fixed point M_3 when the latter is stable and by the period of the limit cycle and the relaxation time toward it when M_3 is unstable.

III. STOCHASTIC ROSENZWEIG-MACARTHUR MODEL: EXTINCTION FROM A LIMIT CYCLE

A. Two routes to extinction

How does the deterministic picture change when one accounts for the stochasticity of the elemental processes of the RMA model and the discrete character of the population sizes? Figure 2 shows a stochastic realization of the RMA model in the R, F plane. As one can see, at sufficiently large N and at intermediate times, the stochastic trajectory closely follows the deterministic one. The long-time behavior, however, is
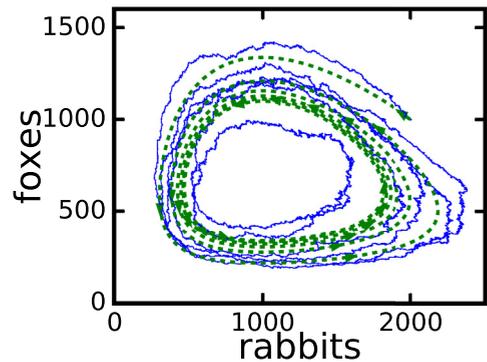
FIG. 2. Phase-space trajectories of the deterministic RMA model (dashed line) vs a Monte Carlo simulation of the stochastic model (solid line). Parameters are $a = 1$, $\sigma = 3.2$, $\tau = 0.5$, and $N = 1600$. For intermediate times, the stochastic dynamics closely follow the deterministic dynamics. For much longer times (not shown), at least one of the populations goes extinct (see Fig. 3).
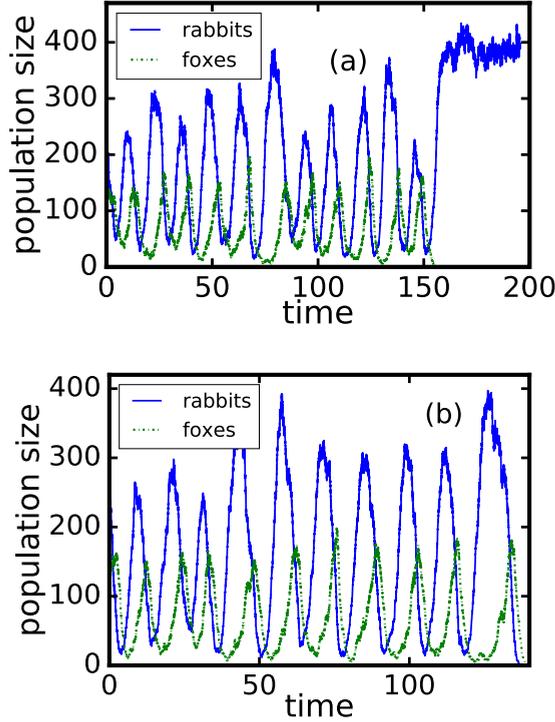
FIG. 3. Two stochastic realizations of the RMA model for $a = 1$, $\tau = 0.5$, $\sigma = 3.2$, and $N = 192$. Shown are the population sizes of rabbits (solid lines) and foxes (dashed lines) versus time. (a) Foxes go extinct first, whereas rabbits approach a steady state around the fixed point M_2 and live on forever. (b) Rabbits go extinct first, at $t \simeq 137$, and foxes go extinct very soon afterwards, at $t \simeq 142$.

dramatically different: At least one of the populations here goes extinct, and this happens in one of two possible ways. Figures 3(a) and 3(b) show two stochastic realizations for the same values of parameters [which coincide with those in Fig. 1(b)] and for the same initial conditions. In Fig. 3(a) the foxes go extinct, while the rabbit population approaches a nonzero steady state. In Fig. 3(b) the rabbits go extinct first, followed by a quick extinction of the foxes. The population extinction results from the presence of two absorbing states in this system: the empty state and the state without foxes but with a nonzero rabbit population. (Note that, in our model, the rabbits are immortal in the absence of foxes.) One of these two absorbing states is always ultimately reached. At $N \gg 1$ this usually happens due to a rare large fluctuation when starting from the long-lived population state in the vicinity of the deterministic limit cycle.

B. Master equation and long-time dynamics

Let $P_{m,n}(t)$ be the probability of finding m rabbits and n foxes in the system at time t. The dynamics of $P_{m,n}(t)$ is governed by the master equation,

$$
\begin{aligned}
\dot{P}_{m,n} = \hat{H} P_{m,n} &= a[(m-1)P_{m-1,n} - m P_{m,n}] \\
&+ \frac{\sigma(m+1)(n-1)}{N + \sigma\tau(m+1)} P_{m+1,n-1} - \frac{\sigma mn}{N + \sigma\tau m} P_{m,n} \\
&+ (n+1)P_{m,n+1} - n P_{m,n} \\
&+ (1/2N)[(m+1)m P_{m+1,n} - m(m-1)P_{m,n}], \quad (8)
\end{aligned}
$$

where $P_{m,n} = 0$ when any of the indices is negative. At times much longer than t_r but shorter than the MTE (see below), a quasistationary distribution appears around the deterministic limit cycle [9]. Following Ref. [10], we can define the *effective probability contents* of the vicinities of the fixed points M_1, M_2 and the limit cycle:

$$
\mathcal{P}_1(t) = P_{0,0}(t), \tag{9}
$$

$$
\mathcal{P}_2(t) = \sum_{m=1}^{\infty} P_{m,0}(t), \tag{10}
$$

$$
\mathcal{P}_3(t) = \sum_{m=1}^{\infty} \sum_{n=1}^{\infty} P_{m,n}(t). \tag{11}
$$

Assuming $N \gg 1$ and $t \gg t_r$, the main contributions to the sums in Eqs. (10) and (11) come from the close vicinities of the fixed point M_2 and the limit cycle, respectively. The effective long-time dynamics of $\mathcal{P}_1$, $\mathcal{P}_2$, and $\mathcal{P}_3$ are given by a three-state master equation [10],

$$
\begin{aligned}
\dot{\mathcal{P}}_1(t) &= \mathcal{R}_1 \mathcal{P}_3(t), \\
\dot{\mathcal{P}}_2(t) &= \mathcal{R}_2 \mathcal{P}_3(t), \\
\dot{\mathcal{P}}_3(t) &= -(\mathcal{R}_1 + \mathcal{R}_2)\mathcal{P}_3(t),
\end{aligned}
\tag{12}
$$

where $\mathcal{R}_1$ and $\mathcal{R}_2$ are the extinction rates along the first and second extinction routes, respectively. At $t \gg t_r$, we assume that initially the populations occupy the coexistence state in the vicinity of the limit cycle:

$$
[\mathcal{P}_1(0), \mathcal{P}_2(0), \mathcal{P}_3(0)] = (0, 0, 1). \tag{13}
$$

Then the solution of Eq. (12) is [10]

$$
\mathcal{P}_1(t) = \frac{\mathcal{R}_1 [1 - e^{-(\mathcal{R}_1 + \mathcal{R}_2)t}]}{\mathcal{R}_1 + \mathcal{R}_2}, \tag{14}
$$

$$
\mathcal{P}_2(t) = \frac{\mathcal{R}_2 [1 - e^{-(\mathcal{R}_1 + \mathcal{R}_2)t}]}{\mathcal{R}_1 + \mathcal{R}_2}, \tag{15}
$$

$$
\mathcal{P}_3(t) = e^{-(\mathcal{R}_1 + \mathcal{R}_2)t}. \tag{16}
$$

As one can see from Eqs. (14)–(16), the long-term behavior of the system is determined by the extinction rates $\mathcal{R}_1$ and $\mathcal{R}_2$. Their evaluation, therefore, is our main objective.

From Eqs. (14)–(16), the mean time to extinction of foxes is [10]

$$
\begin{aligned}
\text{MTE}_F &= \int_0^{\infty} dt\, t \big[\dot{P}_1(t) + \dot{P}_2(t)\big] = -\int_0^{\infty} dt\, t\, \dot{P}_3(t) \\
&= 1/(\mathcal{R}_1 + \mathcal{R}_2),
\end{aligned}
\tag{17}
$$

whereas the mean time to extinction of the rabbits is formally infinite. As we see below, the first extinction scenario is much less likely than the second, i.e., $\mathcal{R}_1 \ll \mathcal{R}_2$. As a result, the MTE of the foxes can be approximated as

$$
\text{MTE}_F \simeq 1/\mathcal{R}_2. \tag{18}
$$

We now briefly discuss, for completeness, how the extinction rates are encoded in the spectrum of the linear operator $\hat{H}$, introduced in Eq. (8). Let us denote the eigenvalues and eigenstates of $\hat{H}$ by λ_i and $\pi_{m,n}^{(i)}$, respectively, i.e.,

$$
\hat{H} \pi_{m,n}^{(i)} = -\lambda_i \pi_{m,n}^{(i)}. \tag{19}
$$

We can write the solution of the time-dependent master equation, (8), in terms of the eigenstates as

$$P_{m,n}(t) = \sum_{i=1}^{\infty} C_i \pi_{m,n}^{(i)} e^{-\lambda_i t}, \qquad (20)$$

where the constants C_i are determined by the initial condition $P_{m,n}(0)$ [10]. Two of the eigenstates describe the (truly) steady-state solutions, corresponding to the empty state and the fox-free state with a steady-state population of rabbits. Their corresponding eigenvalues are both equal to 0. The smallest nonzero eigenvalue is $\lambda_3 = \mathcal{R}_1 + \mathcal{R}_2$ [10].

Our principal task in the remainder of this paper is to evaluate this eigenvalue and the extinction rates $\mathcal{R}_1$ and $\mathcal{R}_2$ by examining the eigenvalue problem,

$$\hat{H}\pi_{m,n} = -(\mathcal{R}_1 + \mathcal{R}_2)\pi_{m,n}, \quad n > 0. \qquad (21)$$

Since the extinction rates are exponentially low in $N \gg 1$, one can approximate the full Eq. (19) for $\pi_{m,n}$ by the quasistationary equation

$$\hat{H}\pi_{m,n} \simeq 0, \quad m > 0, \quad n > 0. \qquad (22)$$

C. WKB approximation

1. General

For $N \gg 1$, Eq. (22) can be approximately solved via the WKB ansatz [27],

$$\pi_{m,n} = \exp[-NS(x,y)], \qquad (23)$$

where $x = m/N$ and $y = n/N$. Assuming that $S(x,y)$ is a smooth function of x and y, we plug this ansatz into Eq. (22) and Taylor-expand S around (x,y). In the leading order in $1/N$, this procedure yields a zero-energy Hamilton-Jacobi equation, $H(x,y,\partial_x S,\partial_y S) = 0$, with the effective Hamiltonian

$$H(x,y,p_x,p_y) = ax(e^{p_x} - 1) + \frac{\sigma xy}{1 + \sigma\tau x}(e^{p_y - p_x} - 1)$$
$$+ y(e^{-p_y} - 1) + \frac{x^2}{2}(e^{-p_x} - 1). \qquad (24)$$

The Hamilton equations are

$$\dot{x} = axe^{p_x} - \frac{x^2}{2}e^{-p_x} - \frac{\sigma xy}{1 + \sigma\tau x}e^{p_y - p_x},$$

$$\dot{y} = \frac{\sigma xy}{1 + \sigma\tau x}e^{p_y - p_x} - ye^{-p_y},$$

$$\dot{p}_x = a(1 - e^{p_x}) + x(1 - e^{-p_x}) + \frac{\sigma y}{(1 + \sigma\tau x)^2}(1 - e^{p_y - p_x}),$$

$$\dot{p}_y = (1 - e^{-p_y}) + (1 - e^{p_y - p_x})\frac{\sigma x}{1 + \sigma\tau x}. \qquad (25)$$

We are only interested in the zero-energy manifold $H = 0$. Note that in the zero-energy invariant hyperplane $p_x = p_y = 0$, the dynamics of x and y reduce to the deterministic dynamics, (3). Therefore, the three deterministic fixed points, $M_1 = (0,0,0,0)$, $M_2 = (2a,0,0,0)$, and $M_3 = (x^*,y^*,0,0)$ are also fixed points of the Hamiltonian dynamics, (25). In its turn, the deterministic limit cycle is an exact time-periodic solution of the Hamilton equations, (25), with $p_x = p_y = 0$.

In addition, there are two "fluctuational" fixed points:

$$F_1 = (0,0,-\infty,0),$$
$$F_2 = \left[2a,0,0,\ln\left(\frac{1 + 2a\tau\sigma}{2a\sigma}\right)\right]. \qquad (26)$$

Fluctuational fixed points have a nonzero p_x or p_y component and appear in a whole class of stochastic population models that exhibit extinction in the absence of an Allee effect [1–4,31].

We can evaluate the extinction rates $\mathcal{R}_1$ and $\mathcal{R}_2$ by evaluating the QSD $\pi_{m,n}$ at $(x = 0, y = 0)$ and $(x = 2a, y = 0)$, respectively. This is done by calculating the actions S_1 and S_2 along the corresponding instantons: phase-space trajectories which begin, at $t = -\infty$, in the deterministic limit cycle and end, at $t = \infty$, at the fluctuational fixed points F_1 and F_2, respectively. These actions are

$$S_1 = \int_{(x_{lc},y_{lc})}^{F_1} p_x dx + p_y dy \quad \text{and}$$

$$S_2 = \int_{(x_{lc},y_{lc})}^{F_2} p_x dx + p_y dy.$$

With exponential accuracy, the extinction rates $\mathcal{R}_1$ and $\mathcal{R}_2$ are [10]

$$\mathcal{R}_1 \sim \exp(-NS_1), \quad \mathcal{R}_2 \sim \exp(-NS_2). \qquad (27)$$

2. Some properties of the instantons. Shooting method

For the case of extinction from a fixed point, the instantons can be found numerically: either by shooting [3,4,10] or by iterating the equations for $\dot{x}$ and $\dot{y}$ forward in time and the equations for $\dot{p}_x$ and $\dot{p}_y$ backward in time [8,31,32]. Here we modify the shooting method [3,4,10] to make it suitable for an instanton which exits, at $t = -\infty$, a deterministic limit cycle and enters, at $t = \infty$, one of the fluctuational fixed points. First, we need to discuss some important properties of such instantons. In particular, how the instanton exits the limit cycle is crucial for the shooting method we present.

In the case of extinction from an attracting fixed point, one proceeds by linearizing the Hamilton equations near the fixed point and finding the unstable eigenvectors of the linearizing matrix. The matrix will have two "stable" (deterministic) eigenvectors and two "unstable" eigenvectors, whose eigenvalues have a positive real part (see, e.g., Eq. (7.25) in Ref. [33]). The instanton (which, in this case, is a heteroclinic trajectory going to a fluctuational fixed point) is then found by looking for a linear combination of the two unstable eigenvectors of a fixed (and very small) norm, using the shooting method [3,4].

When the extinction is from a stable limit cycle, the leading-order dynamics in the vicinity of the limit cycle is best described by Floquet theory (see, e.g., [34]). For each point $\boldsymbol{v}_{lc} = (x_{lc}, y_{lc}, 0, 0)$ in the limit cycle, we define its Floquet matrix $\mathbb{B}$ as follows: Given a starting point which is near the limit cycle, $\boldsymbol{v}_{lc} + \boldsymbol{\delta v}$, and advancing in time according to the Hamilton equations, we will arrive, after one period of the limit cycle, at the point $\boldsymbol{v}_{lc} + \mathbb{B}\boldsymbol{\delta v} + O(\|\boldsymbol{\delta v}\|^2)$. The eigenvectors and eigenvalues of the Floquet matrix will determine the stable and unstable directions in phase space. (We assume everywhere in the following that the eigenvectors

are normalized to unity.) Although the Floquet matrix $\mathbb{B}$ itself and its eigenvectors are local quantities which vary along the limit cycle, its eigenvalues are independent of the choice of the point $(x_{lc}, y_{lc}, 0, 0)$ in the limit cycle [33,34].

As in the fixed-point case, $\mathbb{B}$ will have two "deterministic" (zero-momentum) eigenvectors. The corresponding eigenvalues will be λ and 1. $\lambda < 1$ corresponds to a stable eigenvector, and 1 corresponds to a neutral eigenvector, which is tangent to the limit cycle at its every point. Note that λ must be positive; otherwise, phase-space trajectories would cross each other. The two additional eigenvalues of $\mathbb{B}$ must be equal to 1 (another neutral eigenvector) and $1/\lambda$ (an unstable eigenvector) (see Eq. (7.27) in Ref. [33] or Ref. [35] for the proof). Therefore, there is only *one* unstable direction through which a trajectory can exit the limit cycle. We now understand how the instanton exits the limit cycle. It starts in the limit cycle at $t = -\infty$ and then performs an infinite number of rotations around the limit cycle, each one farther from the limit cycle by a factor of $1/\lambda$, before departing.

In view of this basic property of the instanton, our numerical method consists of several steps. The first step is to choose an arbitrary point $\boldsymbol{v_{lc}} = (x_{lc}, y_{lc}, 0, 0)$ in the limit cycle. This is done by numerically integrating the deterministic equations, (3). The period T of the limit cycle is computed numerically as well.

We then numerically compute the Floquet matrix $\mathbb{B}$ at the point $\boldsymbol{v_{lc}}$ we chose. This is done by adding small perturbations to each of the four coordinates of $\boldsymbol{v_{lc}}$ in turn and then advancing the Hamiltonian equations, (25), from time $t = 0$ to $t = T$. The result is a point which is near $\boldsymbol{v_{lc}}$, but the small distance from it gives us a column of the Floquet matrix. For example, we set $\boldsymbol{u}(t = 0) = (x_{lc}, y_{lc}, \delta p_x, 0)$ and then advance $\boldsymbol{u}(t)$ according to the Hamilton equations, until time $t = T$. The third column in the Floquet matrix is then given by $[\boldsymbol{u}(t = T) - \boldsymbol{v_{lc}}]/\delta p_x + O(\delta p_x)$.

Next we diagonalize the Floquet matrix and find its only unstable vector $\boldsymbol{v}$, whose eigenvalue $1/\lambda$ is larger than 1. Since the instanton must exit the limit cycle through this unstable direction, we expect there to be a discrete set of ϵ's for which $\boldsymbol{v_{lc}} + \epsilon\boldsymbol{v}$ is on the instanton (to leading order in ϵ). What is left is to find one such ϵ by the shooting method. We emphasize that ϵ can be taken to be as small as we like, because if $\boldsymbol{v_{lc}} + \epsilon\boldsymbol{v}$ is on the instanton, then so is $\boldsymbol{v_{lc}} + \lambda\epsilon\boldsymbol{v}$ to leading order in ϵ.

It is easy to show that $\partial H/\partial v \equiv \nabla H \cdot \boldsymbol{v}$, the derivative of the Hamiltonian H in the direction of the unstable eigenvector $\boldsymbol{v}$, vanishes. Let us start from some initial condition

$$\boldsymbol{u}(t = 0) = \boldsymbol{u_0} = (x_{lc}, y_{lc}, 0, 0) + \epsilon\boldsymbol{v}.$$

Assuming that ϵ is small enough, $\epsilon \ll 1$, the energy at this point is $H(u_0) \simeq \epsilon\,\partial H/\partial v$. After advancing the Hamiltonian dynamics by the period T of the limit cycle, the system will be at the point

$$\boldsymbol{u}(t = T) \simeq (x_{lc}, y_{lc}, 0, 0) + \lambda^{-1}\epsilon\boldsymbol{v},$$

and the energy will be

$$H[\boldsymbol{u}(t = T)] \simeq \lambda^{-1}\epsilon\frac{\partial H}{\partial \boldsymbol{v}}.$$
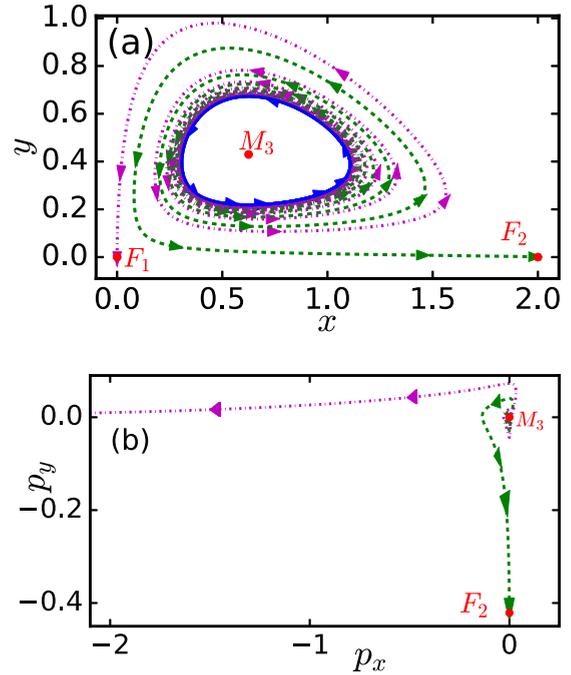
FIG. 4. Numerically found instantons from the stable limit cycle (solid line) to F_1 (dot-dashed line) and to F_2 (dashed line). Parameters are $a = 1$, $\sigma = 3.2$, and $\tau = 0.5$. (a) The xy projections; (b) the $p_x p_y$ projections.

By virtue of energy conservation,

$$H[\boldsymbol{u}(t = T)] = H(\boldsymbol{u_0}).$$

Since λ is different from 1 ($\lambda < 1$), this implies that $\partial H/\partial v = 0$.

As we see now, there are three directions which are tangent to the zero-energy manifold: the two deterministic directions and the unstable direction $\boldsymbol{v}$. Is the fourth direction—the neutral "quantum" eigenvector—also tangent to the zero-energy manifold? The answer is no. The reason is that, in the limit cycle, $\nabla H \neq 0$ (the gradient of H vanishes only at fixed points of the Hamiltonian dynamics), so there cannot be four independent directions for which the directional derivative is 0.

3. Finding the instantons and evaluating S_1 and S_2

Examples of numerically found instantons which start at the limit cycle and end at the fluctuational fixed points F_1 and F_2 are shown in Fig. 4. Figure 5 compares the extinction rates $\mathcal{R}_i$ obtained by solving numerically the (truncated) master equation, (8), with the result of the leading-order WKB approximation, e^{-NS_i}. The truncation of the master equation is done by introducing a sufficiently large artificial cutoff size for the populations, as described in [9]. Figure 6 shows our results for the the mean time to extinction of foxes MTE_F and for the ratio of the probabilities of the two extinction routes, $\mathcal{P}_1/\mathcal{P}_2$, obtained by averaging over many Monte Carlo simulations. The same figure shows the corresponding leading-order WKB predictions $1/(e^{-NS_1} + e^{-NS_2}) \simeq e^{NS_2}$ and $e^{N(S_2-S_1)}$. In both cases a good agreement, up to undetermined WKB prefactors, is observed between the numerical and the WKB results. We investigate the prefactors in Sec. IIIC5.
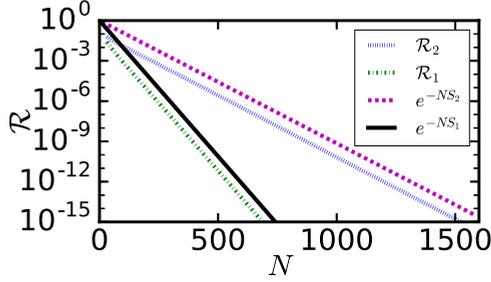
FIG. 5. Extinction rates $\mathcal{R}_i$, determined by solving the master equation, (8), numerically for different N's, are compared with the extinction rates e^{-NS_i} calculated in the leading-order WKB approximation. Parameters are $a = 1$, $\tau = 0.5$, and $\sigma = 3.1$. The actions along the instantons are $S_1 \simeq 0.0466$ and $S_2 \simeq 0.0211$. Vertical shifts are due to the undetermined WKB prefactors $\mathcal{F}_1$ and $\mathcal{F}_2$ (see Sec. IIIC5).

4. Nonanalytic behavior of the entropic barrier near the Hopf bifurcation

Figure 7 presents our numerical results for the actions $S_{1,2}$ calculated along the instantons leading to F_1 and F_2, respectively, for the same $a = 1$ and $\tau = 0.5$ and different values of σ close to the Hopf bifurcation, $\sigma = \sigma^*$. For $\sigma < \sigma^*$ the fixed point M_3 is stable, and the actions were calculated on the instantons which start at M_3. An immediate observation is that $S_1 > S_2$ for all σ, so that the effective transition rate $\mathcal{R}_2$ is *exponentially* greater than $\mathcal{R}_1$, as observed previously for extinction from a fixed point [10]. The (numerically evaluated) first derivatives of the entropic barriers with respect to σ are also shown as functions of σ [Figs. 7(b) and 7(d)]. Interestingly, the first derivatives exhibit corner singularities at $\sigma = \sigma^*$ indicating jumps in the second derivatives (so the phenomenon can be classified as a dynamic second-order phase transition).

Let us now consider a simple toy model of a "noisy" Hopf bifurcation that displays qualitatively the same phenomenon but can be solved analytically. The model is defined by two
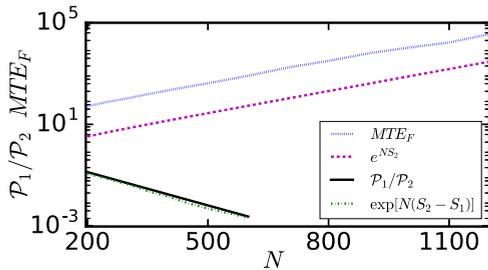
FIG. 6. N dependence of the mean time to extinction of the foxes MTE_F and of the ratio of probabilities of the two extinction scenarios $\mathcal{P}_1/\mathcal{P}_2$ for fixed $a = 1$, $\tau = 0.5$, and $\sigma = 4$. Results obtained by averaging over many Monte Carlo simulations are compared with leading-order WKB predictions. Values are plotted on a semilog scale. The actions are $S_1 \simeq 0.0167$ and $S_2 \simeq 0.00665$. Since $S_2 < S_1$, the MTE of the foxes is approximated in the WKB theory as $\mathrm{MTE}_F \simeq e^{NS_2}$ [see Eq. (18)]. Vertical shifts are due to the undetermined WKB prefactors $\mathcal{F}_i$ (see Sec. IIIC5).

Langevin equations in polar coordinates,

$$\dot{r} = \alpha r - \beta r^3 + \gamma r^5 + \epsilon \xi(t), \quad \dot{\theta} = 1, \qquad (28)$$

where $\xi(t)$ is zero-mean Gaussian noise, delta-correlated in time. As the equations for r and θ are decoupled, the problem is effectively one-dimensional. We assume that β and γ are positive and examine the Hopf bifurcation which occurs when α changes sign. Close to the bifurcation $|\alpha| \ll 1$. We consider the weak-noise limit, $\epsilon \to 0$, and assume that the noise is smaller than the rest of the parameters, including $|\alpha|$.

The equation for r can be written in the form $\dot{r} = -V'(r) + \epsilon \xi(t)$, where we have defined the deterministic potential

$$V(r) = -\frac{\alpha}{2} r^2 + \frac{\beta}{4} r^4 - \frac{\gamma}{6} r^6 \qquad (29)$$

(see Fig. 8).

In the toy model, the mean escape time (MET) from the metastable state near the origin $r_{\min}$ is given by Kramers' formula [36]. To leading order, $\ln(\mathrm{MET}) \simeq 2\Delta V/\epsilon^2$, where $\Delta V = V(r_{\max}) - V(r_{\min})$ is the height of the potential barrier, $r_{\max}$ is the global maximum of V, and $r_{\min}$ is the coordinate of the metastable state near the origin (see Fig. 8). The quantities ΔV and $1/\epsilon^2$ are analogous to the action S and the characteristic population size N, respectively, in the stochastic RMA model.

For $\alpha < 0$, the origin is a stable fixed point of the deterministic dynamics and a local minimum of V, so $r_{\min} = 0$ and $V(r_{\min}) = 0$. For $\alpha > 0$, the origin is unstable, and a limit cycle appears around it, of radius $r_{\min} \simeq \sqrt{\alpha/\beta}$. Now the local minimum of the potential is $V(r_{\min}) \simeq -\alpha^2/(4\beta)$, where we have assumed that $r_{\min} \ll 1$, which holds near the bifurcation.

If we now consider ΔV as a function of α, we can easily see that it is nonanalytic at $\alpha = 0$, because of the nonanalytic behavior of $V(r_{\min})$. From the expressions for $V(r_{\min})$ below and above the bifurcation, we find that the second derivative $\partial^2 \Delta V/\partial \alpha^2$ jumps by $1/(2\beta)$.

This prediction from the toy model is quite general and depends only on the behavior of the potential near the origin. In particular, the value (and even the sign) of γ in Eq. (29) does not affect the results in any way: all that matters is that higher order terms in r guarantee the existence of a finite $r_{\max}$.

The prediction of nonanalytic behavior at the Hopf bifurcation can be extended to the stochastic RMA model. Near the bifurcation, and in the vicinity of M_3 and/or the limit cycle around it, the Fokker-Planck approximation of the master equation, (8), is applicable and can be obtained by the van Kampen system-size expansion [36]. After rescaling the coordinates, a radial Langevin equation can be deduced, and it is of the same form as Eq. (28). However, the amount by which $\partial^2 S_i/\partial\sigma^2$ jumps in the stochastic RMA model is in disagreement with the prediction of the toy model. To begin with, the jumps of the second derivatives for S_1 and S_2 are, in general, not equal to each other, as clearly shown in Fig. 7. The reason for the disagreement is that, in a nonequilibrium system like the stochastic RMA model, the actions S_1 and S_2, and therefore the jumps in their second derivatives with respect to the σ, are affected by the variation along the entire instantons. Therefore, the toy model misses one crucial
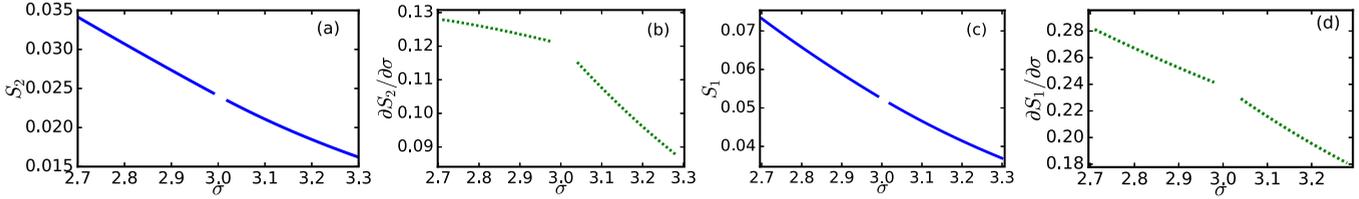
FIG. 7. Jumps in the second derivatives of the entropic barriers to extinction with respect to the bifurcation parameter σ at the Hopf bifurcation. Solid lines: the actions (a) S_2 and (c) S_1 along the instantons. Dashed lines: the first derivatives (b) $\partial S_2/\partial\sigma$ and (d) $\partial S_1/\partial\sigma$. The actions and their first derivatives are continuous, while the second derivatives are discontinuous at the Hopf bifurcation. Parameters are $a = 1$, $\tau = 0.5$. The Hopf bifurcation occurs at $\sigma^* = 3$ [see Eq. (7)].

feature of the stochastic RMA model: its nonequilibrium character.

5. Prefactors of the extinction rates

We now study the prefactors $\mathcal{F}_1$ and $\mathcal{F}_2$, which are the subleading corrections to the extinction rates $\mathcal{R}_i = \mathcal{F}_i e^{-NS_i}$, $i = 1,2$, at $N \gg 1$. Our numerical results for the dependence of the prefactors on N (for fixed a, σ, and τ) are shown in Fig. 9. One can see an apparent power-law dependence, whose exponent changes at the Hopf bifurcation $\sigma = \sigma^*$. We observed the same behavior for other sets of a, σ, τ as well (not shown). When the fixed point M_3 is attracting, the prefactors appear to behave as $\mathcal{F} \propto N^{1/2}$. For a stable limit cycle, they appear to be independent of N.

How can we interpret these numerical results? For multipopulation systems the prefactors cannot, in general, be found analytically. It is natural to assume, however, that the prefactors depend on $N \gg 1$ as a power law, $\mathcal{F} \propto N^\mu$. Indeed, apart from our numerical results for the RMA model, power-law behaviors of the prefactors of the extinction rates have been observed in all cases where the prefactors could be calculated analytically: for single populations [2,37–39] and for two-population systems which possess a time-scale separation [6].

We now propose a simple argument which explains why the exponent of the power law μ changes by 1/2 at the Hopf bifurcation, as evidenced by Fig. 9. The argument is based on the normalization of the quasistationary distribution π_{mn}, which is strongly affected by the Hopf bifurcation.

When M_3 is a stable fixed point, the quasistationary distribution π_{mn} in the vicinity of M_3 is a two-dimensional Gaussian peaked at M_3, with standard deviations of order $\sqrt{N}$ in either direction. This part of the distribution gives the main contribution to the normalization. The value of the quasistationary distribution function at its peak is therefore of order $\pi_{m^*n^*} \sim 1/N$, where $(m^*, n^*) = (Nx^*, Ny^*)$ is the fixed point M_3.

In the case of a limit cycle, the distribution π_{mn} is well approximated by a Gaussian "ridge" around the limit cycle, whose width is of order $\sqrt{N}$ [40]. Since the length of the limit cycle increases linearly with N, the value of the quasistationary distribution function in the limit cycle is of order $\pi(m_{lc}, n_{lc}) \sim N^{-3/2}$. This will in turn add a factor of order $N^{-1/2}$ to the whole distribution π_{mn}, compared to the fixed-point case. We therefore expect the prefactor's power-law dependence on N to change at the bifurcation, and the exponent μ to drop by 1/2 at the Hopf bifurcation, as Fig. 9 indeed suggests.

IV. CONCLUSIONS

We have studied population extinction from a limit cycle due to intrinsic noise in the Rosenzweig-MacArthur model. In the leading-order WKB approximation, the calculation of the extinction rates and the most probable extinction paths boils down to finding a new type of instanton of an effective Hamiltonian system. We have developed a numerical method of computing these instantons. The method is based
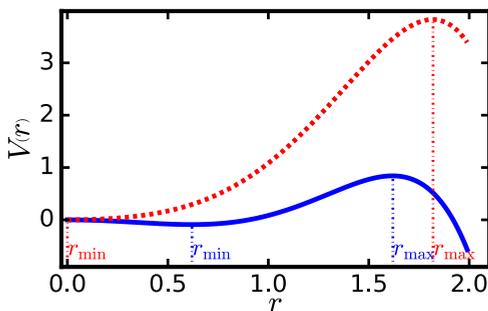
FIG. 8. Deterministic potential, (29), of the toy model. Parameters are $\beta = 3, \gamma = 1$, and $\alpha = 1$ (solid line) or $\alpha = -1$ (dashed line). $r_{\min}$ and $r_{\max}$ are labeled. The Hopf bifurcation is at $\alpha = 0$, where $r_{\min}$ changes from 0 to a positive value. Close to the bifurcation $|\alpha| \ll 1$. However, for clarity of the figure we used values of α which are not small.
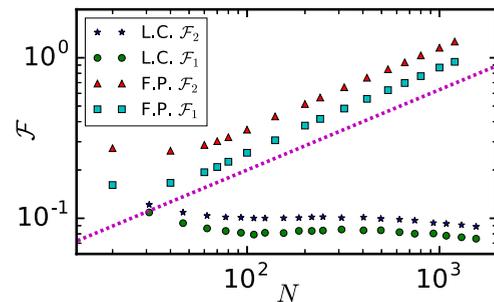
FIG. 9. N dependence of the numerically evaluated prefactors $\mathcal{F}_i(a,\sigma,\tau,N)$ ($i = 1,2$) for fixed $a = 1$, $\tau = 0.5$, and $\sigma = 3.1$ (limit cycle; L.C.) or $\sigma = 2$ (fixed point; F.P.). For $N \gg 1$, there is an apparent power-law dependence on N, whose exponent changes at the bifurcation. For a fixed point, the prefactor scales as $\mathcal{F} \propto N^{1/2}$, while for a limit cycle it appears to be independent of N. The dashed line has a slope of 1/2 and is a guide for the eye.

on Floquet theory and involves numerical determination of the unstable direction in which the instantons exit the limit cycle.

We have shown numerically that the entropic barriers to extinction S_1 and S_2 exhibit a nonanalytic behavior—a second-order dynamic phase transition—at the Hopf bifurcation. We leave as an open problem the challenge of analytically calculating the jump in the second derivative. We believe that there are two contributions to this jump: one is a contribution from the close vicinity of the fixed point M_3 that can be calculated analytically, as we have shown by using a simple toy model. The second contribution comes from the variation of the action due to the global change in the shape of the instanton. This contribution is hard to calculate analytically.

We also obtained numerical results for the extinction rate prefactors: the subleading corrections of the WKB theory. As we found, the prefactors show a power-law dependence on the population size scale N. The exponent of the power law changes at the Hopf bifurcation, and we suggested an explanation of this change in terms of a simple normalization argument.

[1] O. Ovaskainen and B. Meerson, Trends Ecol. Evol. **25**, 643 (2010).

[2] M. Assaf and B. Meerson, Phys. Rev. E **81**, 021116 (2010).

[3] M. I. Dykman, I. B. Schwartz, and A. S. Landsman, Phys. Rev. Lett. **101**, 078101 (2008).

[4] A. Kamenev and B. Meerson, Phys. Rev. E **77**, 061107 (2008).

[5] M. Khasin and M. I. Dykman, Phys. Rev. Lett. **103**, 068101 (2009).

[6] M. Khasin, B. Meerson, and P. V. Sasorov, Phys. Rev. E **81**, 031126 (2010).

[7] M. Khasin, M. I. Dykman, and B. Meerson, Phys. Rev. E **81**, 051925 (2010).

[8] I. Lohmar and B. Meerson, Phys. Rev. E **84**, 051901 (2011).

[9] The Supplemental Material at http://link.aps.org/supplemental/10.1103/PhysRevE.93.032109 includes a video which shows the evolution of $P_{m,n}(t)$ in time well before extinction occurs.

[10] O. Gottesman and B. Meerson, Phys. Rev. E **85**, 021140 (2012).

[11] A. Gabel, B. Meerson, and S. Redner, Phys. Rev. E **87**, 010101(R) (2013).

[12] C. Elton and M. Nicholson, J. Anim. Ecol. **11**, 215 (1942).

[13] L. Butler, Can. J. Zool. **31**, 242 (1953).

[14] A. D. Bazykin, *Nonlinear Dynamics of Interacting Populations* (World Scientific, Singapore, 1998).

[15] E. Odum and G. W. Barrett, *Fundamentals of Ecology* (Cengage Learning, Boston, MA, 2004).

[16] J. D. Murray, *Mathematical Biology: I. An Introduction* (Springer, New York, 2008).

[17] A. J. Lotka, Proc. Natl. Acad. Sci. USA **6**, 410 (1920).

[18] V. Volterra, Mem. Accad. Naz. Lincei **2**, 31 (1926).

[19] M. L. Rosenzweig and R. H. MacArthur, Am. Nat. **97**, 209 (1963).

[20] M. Bartlett, *Stochastic Population Models in Ecology and Epidemiology* (Methuen, London, 1960).

[21] R. Anderson, *Infectious Diseases of Humans: Dynamics and Control* (Oxford University Press, Oxford, UK, 1991).

[22] H. Andersson and T. Britton, *Stochastic Epidemic Models and their Statistical Analysis* (Springer, New York, 2000).

[23] D. Kirschner and J. C. Panetta, J. Math. Biol. **37**, 235 (1998).

[24] A. D'Onofrio and A. Gandolfi, Math. Med. Biol. **26**, 63 (2009).

[25] F. Schlögl, Z. Phys. **253**, 147 (1972).

[26] N. Van-Kampen, *Stochastic Processes in Physics and Chemistry*, 3rd ed. (North-Holland, Amsterdam, 2007).

[27] M. I. Dykman, E. Mori, J. Ross, and P. M. Hunt, J. Chem. Phys **100**, 5735 (1994).

[28] D. M. Roma, R. A. O'Flanagan, A. E. Ruckenstein, A. M. Sengupta, and R. Mukhopadhyay, Phys. Rev. E **71**, 011902 (2005).

[29] K. Cheng, SIAM J. Numer. Anal. **12**, 541 (1981).

[30] H. L. Smith (unpublished); https://math.la.asu.edu/~halsmith/Rosenzweig.pdf.

[31] V. Elgart and A. Kamenev, Phys. Rev. E **70**, 041106 (2004).

[32] A. I. Chernykh and M. G. Stepanov, Phys. Rev. E **64**, 026306 (2001).

[33] P. Cvitanović, R. Artuso, R. Mainieri, G. Tanner, G. Vattay, N. Whelan, and A. Wirzba, *Chaos: Classical and Quantum* (Niels Bohr Institute, Copenhagen, 2012); http://ChaosBook.org.

[34] M. J. Ward, Basic Floquet theory; http://www.emba.uvm.edu/~jxyang/teaching/Floquet_theory_Ward.pdf.

[35] N. R. Smith, M.Sc. thesis, Hebrew University of Jerusalem, Jerusalem (2015), http://hufind.huji.ac.il/Record/HUJ001979466.

[36] C. W. Gardiner, *Handbook of Stochastic Methods for Physics, Chemistry, and the Natural Sciences* (Springer-Verlag, New York, 1985).

[37] M. Assaf and B. Meerson, Phys. Rev. E **74**, 041115 (2006).

[38] D. A. Kessler and N. M. Shnerb, J. Stat. Phys. **127**, 861 (2007).

[39] M. Assaf, B. Meerson, and P. V. Sasorov, J. Stat. Mech. (2010) P07018.

[40] M. I. Dykman, X. Chu, and J. Ross, Phys. Rev. E **48**, 1646 (1993); **52**, 6916 (1995).